



ELSEVIER

Journal of Constructional Steel Research 47 (1998) 193–210

JOURNAL OF
CONSTRUCTIONAL
STEEL RESEARCH

Computational modeling of cold-formed steel: characterizing geometric imperfections and residual stresses

B.W. Schafer*, T. Peköz

School of Civil and Environmental Engineering, Cornell University, Ithaca NY, USA

Received 7 October 1997; received in revised form 12 December 1997; accepted 6 January 1998

Abstract

Thin-walled, cold-formed steel members exhibit a complicated post-buckling regime that is difficult to predict. Today, advanced computational modeling supplements experimental investigation. Accuracy of computational models relies significantly on the characterization of selected inputs. No consensus exists on distributions or magnitudes to be used for modeling geometric imperfections and for modeling residual stresses of cold-formed steel members. In order to provide additional information existing data is collected and analyzed and new experiments performed. Simple rules of thumb and probabilistic concepts are advanced for characterization of both quantities. The importance of the modeling assumptions are shown in the examples. The ideas are summarized in a preliminary set of guidelines for computational modeling of imperfections and residual stresses. © 1998 Elsevier Science Ltd. All rights reserved.

Keywords: Cold-formed steel; Imperfections; Residual stresses; Computational modeling

1. Introduction

Post-buckling of cold-formed steel members is difficult to predict due to material and geometric nonlinearity. Nonetheless, numerical techniques, such as finite element or spline finite strip, have reached a level of maturity such that many are now successfully undertaking ultimate strength analysis of cold-formed steel members

* Corresponding author. Fax: 001-607-2550004

[1–6]. The primary impediment to success is not the mechanics formulation nor the solution method, but rather a fundamental lack of knowledge about the initial state of a cold-formed steel member. Characterization of geometric imperfections and residual stresses is largely unavailable. These fundamental quantities are necessary for reliable completion of advanced analysis and parametric studies of cold-formed steel members.

2. Maximum geometric imperfections

Geometric imperfections refer to deviation of a member from ‘perfect’ geometry. Imperfections of a member include bowing, warping, and twisting as well as local deviations. Local deviations are characterized by dents and regular undulations in the plate. Previous researchers have measured geometric imperfections of cold-formed steel members [4,7–12]. Collected data on geometric imperfections is sorted into two categories: type 1, maximum local imperfection in a stiffened element and type 2, maximum deviation from straightness for a lip stiffened or unstiffened flange (see Fig. 1).

Little detailed information is known about imperfection variation along the length. However, maximum imperfection magnitudes are available. Strength of a cold-formed steel member is particularly sensitive to imperfections in the shape of its eigenmodes. Knowledge of the amplitude of imperfections in the lowest *eigenmodes* is often sufficient to characterize the influential imperfections. Maximum imperfections may be used to provide a conservative estimation of imperfection magnitude in a particular eigenmode.

2.1. Rules of thumb

The following simple rules of thumb apply for width/thickness (w/t) less than 200 for type 1 imperfections and $w/t < 100$ for type 2 imperfections. Thickness should

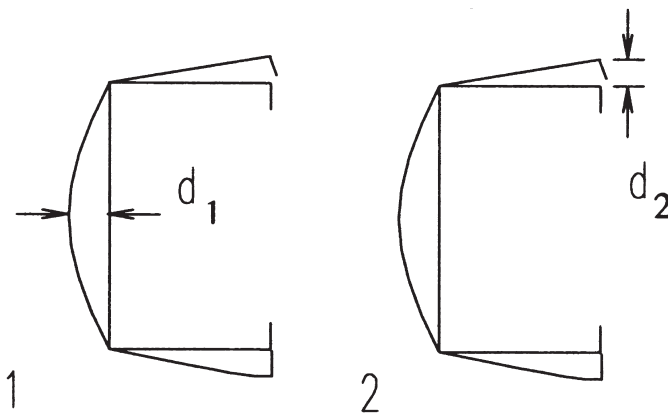


Fig. 1. Definition of geometric imperfections.

be less than 3 mm. For a type 1 imperfection a simple linear regression based on the plate width yields an approximate expression

$$d_1 \approx 0.006w \tag{1}$$

An alternative rule based on an exponential curve fit to the thickness,

$$d_1 \approx 6te^{-2t} \text{ (} d_1 \text{ and } t \text{ in mm)} \tag{2}$$

For type 2 imperfections the maximum deviation from straight is approximately equal to the plate thickness:

$$d_2 \approx t \tag{3}$$

2.2. Probabilistic treatment

Large variation exists in the maximum imperfection data. Simple rules of thumb do not provide a complete characterization of imperfection magnitude. One alternative is to treat the maximum imperfection magnitude as a random variable. Any trend in the data attributed to slenderness or thickness of the plate is now ignored. Histograms of type 1 and type 2 imperfections are given in Fig. 2 and in Fig. 3, respectively. Numerically estimated cumulative distribution function (CDF) values and the summary statistics are given in Table 1.

The CDF values are useful for connecting a probability of occurrence with a parti-

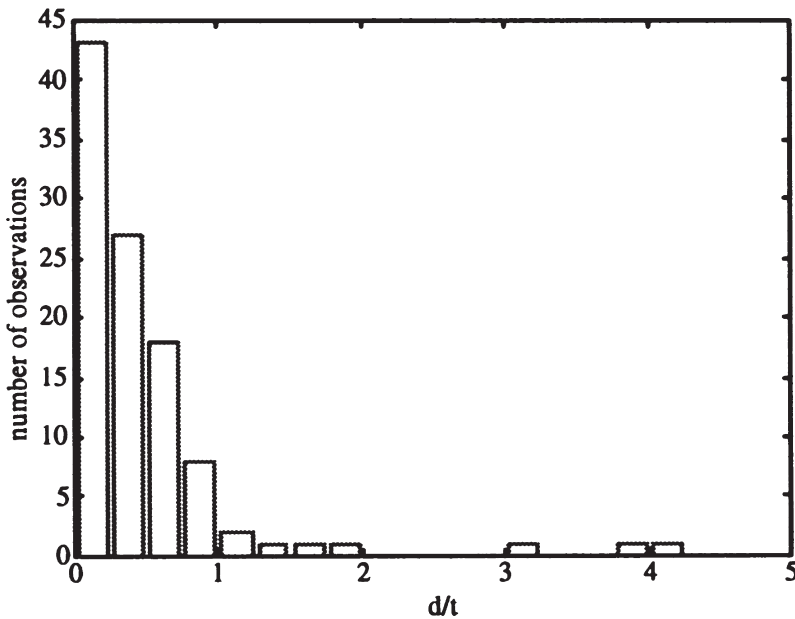


Fig. 2. Histogram of type 1 imperfection.

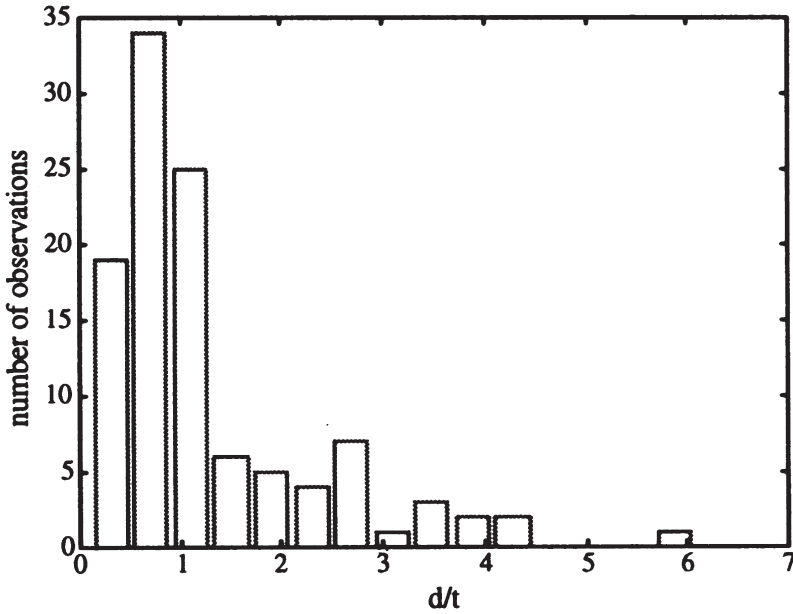


Fig. 3. Histogram of type 2 imperfection.

Table 1
CDF values for maximum imperfection

$P(\Delta < d)$	Type 1	Type 2
	d_1/t	d_2/t
0.25	0.14	0.64
0.50	0.34	0.94
0.75	0.66	1.55
0.95	1.35	3.44
0.99	3.87	4.47
Mean	0.50	1.29
St. dev.	0.66	1.07

cular imperfection magnitude. A CDF value is written as $P(\Delta < d)$ and indicates the probability that a randomly selected imperfection value, Δ , is less than a discrete deterministic imperfection, d . The $P(\Delta < d) = 0.95$ corresponds to a d/t of 1.35 for a type 1 and 3.44 for a type 2 imperfection. A typical member is expected to have maximum imperfections less than these values 95% of the time. General probabilistic approaches using the observed data directly and performing simulation are also possible [13].

3. Geometric imperfections along the length

Existing imperfection data provides only a limited characterization of imperfections. Maximum imperfection data does not give a direct indication of eigenmodes which real imperfections might trigger. True imperfection distributions and magnitude are unknown. To examine actual imperfection distributions and determine what, if any, periodicity exists in the imperfections of real cold-formed steel members a pilot experimental program is undertaken.

3.1. Experimental setup for measurements

Eleven nominally identical specimens are selected for study (see Fig. 4). The basic experimental setup is illustrated in Fig. 5. The specimen is mounted on the table of a milling machine. The milling table provides a flat reference surface for measurement of imperfections. Actual measurement is carried out by replacing the drill bit of the milling machine with a direct current differential transformer (DCDT).

The procedure is automated through the use of the motor which drives the x direction motion of the milling table and by gathering the data in a computer. The DCDT measurements are turned on and recorded in the computer at a constant rate. The milling table motor is then engaged. The table moves at a constant rate for a specified distance. Thus, since the sampling rate is constant and the distance is known, the distance between measurements is known.

3.2. Imperfection signal and transforms

A Fourier transform of the imperfection signal is used to investigate any periodicity in the measured imperfections. The transform reveals both amplitude and fre-

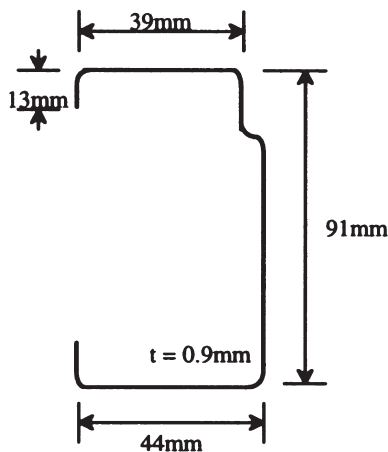


Fig. 4. Nominal geometry.

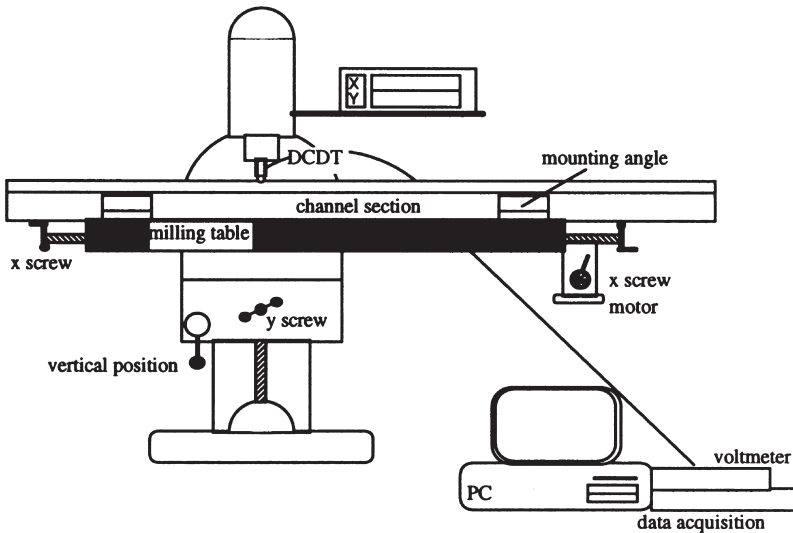


Fig. 5. Experimental setup.

quency of the underlying imperfection. Peaks in the transform plot correspond to dominant sine waves in the imperfection signal.

Post-processing of the raw experimental data is required. Deviation from perfect geometry is approximated by determining a best-fit (least-squares) linear regression line to the raw data and subtracting this line from the raw data. Comparison of the transforms is aided if the spacing of the measurements is equal for the 11 specimens. The original experimental data is sampled at slightly different rates (owing to the rate at which the table moves). The sparsest sampling rate of the 11 specimens governs the sampling rate used in the Fourier transform.

Fig. 6 shows the imperfection signal and Fourier transform for all 11 specimens. The spikes in the signals of specimens 6, 8 and 10 correspond to visible dents in the top flange. Excluding these dents, the imperfection signal is always within ± 1 mm. Despite differences in the signals, the transforms all are relatively similar: one or two low frequency peaks followed by little or no content after 0.005 mm^{-1} . Consistent peaks show that periodicity exists in the imperfection distribution of these members.

3.3. Imperfection spectrum

The imperfection signals all have similar transforms. Thus, an average transform may adequately characterize the imperfection. The 11 individual transforms are averaged to create Fig. 7 — this average or approximated transform is termed an imperfection spectrum. The imperfection spectrum may be used to find the imperfection magnitude in any mode or to generate a complete artificial imperfection pattern.

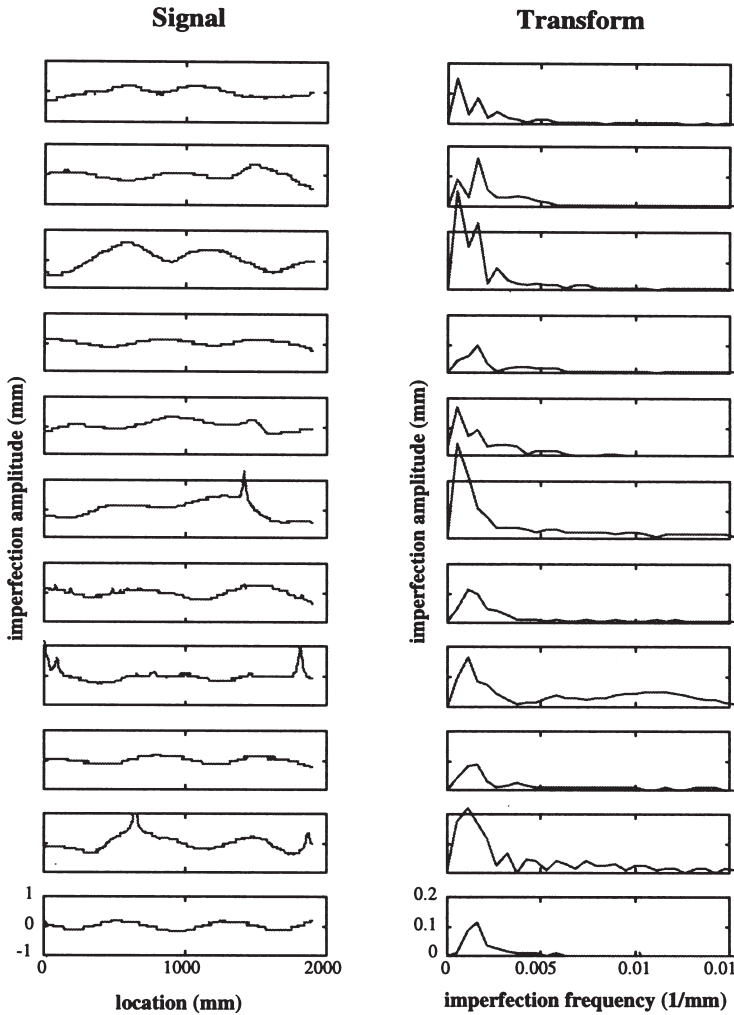


Fig. 6. Imperfection signal and Fourier transform of 11 specimens.

3.4. Modal imperfection magnitudes using imperfection spectrum

The imperfection spectrum may be used to determine the imperfection magnitude in a particular eigenmode — the so-called modal imperfection. Consider a member with sensitivity to a mode with a half-wavelength of 500 mm. This corresponds to an imperfection frequency of $[(500)(2)]^{-1} = 0.001 \text{ mm}^{-1}$ and from the spectrum an imperfection magnitude of approximately 0.11 mm.

The imperfection spectrum allows a quick assessment of the magnitude of imperfection in a particular eigenmode. This is similar to a response spectrum in earthquake engineering where the fundamental vibration modes of a structure can be

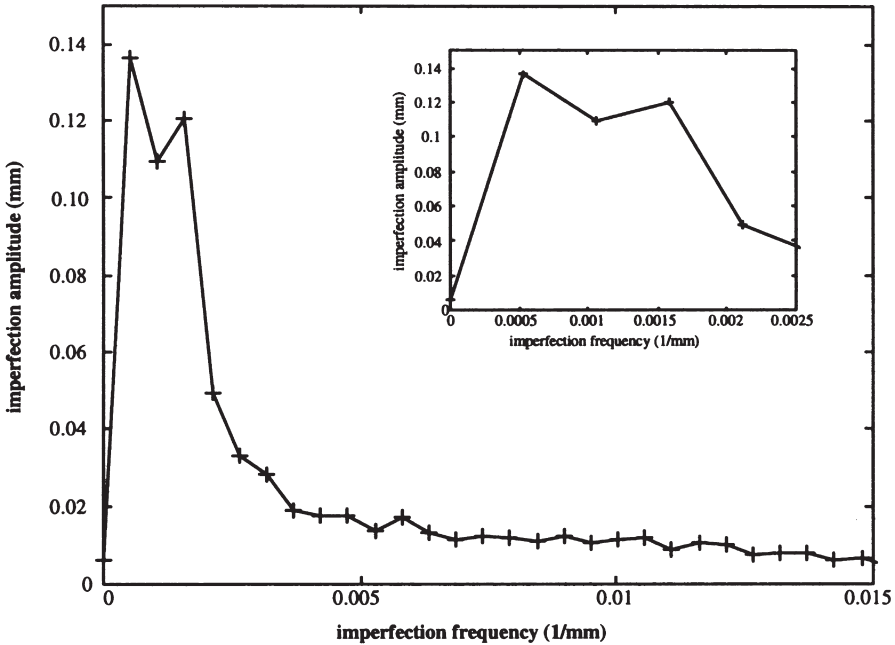


Fig. 7. Average imperfection spectrum.

compared to the frequency content of an earthquake. More work in characterizing typical imperfection spectrums for cold-formed steel members could provide a significant benefit towards understanding the influence of imperfections.

3.5. Generalized imperfections using imperfection spectrum

Just as an earthquake response spectrum may be used to generate artificial earthquake signals, the imperfection spectrum may be used to generate general artificial imperfection signals. General discussion of this type of generation can be found in the literature on random vibrations [14,15]. More specific discussion of this particular application is also available [16]. Consider the generation of an imperfection signal, $X(t)$, where t is the distance along the length of the member. $X(t)$ is a zero-mean, real-valued, stationary Gaussian (normal) process with a given one-sided spectral density. The one-sided spectral density is the previously defined imperfection spectrum with the horizontal axis modified to circular frequency ($\omega = 2\pi f$). The procedure for generating a discrete signal is as follows:

- Determine the form of the imperfection spectrum, for example use Fig. 7.
- Transform the x axis to circular frequency.
- Truncate the spectrum (maximum ω) and discretize it into m pieces.
- Determine the area under each m piece. This area is equal to σ_k^2 .

- Generate m samples of the random variables A_k and B_k . A_k and B_k are independent Gaussian random variables with zero mean and unit variance.
- The imperfection signal is

$$X(t) = \sum_{k=1}^m \sigma_k (A_k \cos \omega_k t + B_k \sin \omega_k t) \tag{4}$$

- Generate new samples of A_k and B_k to create additional imperfection signals.

In addition to theoretical assumptions (e.g. the process is Gaussian) generation of the signal is sensitive to the discretization (m pieces) and to the cutoff frequency (maximum ω). Performing transforms on the generated signals and comparing them to the original spectral density (imperfection spectrum) is a reasonable first approach to test the validity of these assumptions.

4. Residual stresses

Adequate computational modeling of residual stresses is troublesome for analysts. Inclusion of residual stresses (at the integration points of the model for instance) may be complicated. Selecting an appropriate magnitude is made difficult by a lack of data. As a result, residual stresses are often excluded altogether, or the stress–strain behavior of the material is modified to approximate the effect of residual stresses.

In hot-rolled steel members residual stresses do not vary markedly through the thickness, in cold-formed members residual stresses are dominated by a ‘flexural’, or through thickness variation. This variation of residual stresses leads to early yielding on the faces of cold-formed steel plates. This important aspect of the load carrying behavior is completely ignored unless residual stresses are explicitly considered in the analysis.

Experimental work on residual stresses [3,7–10,17,18] includes 16 press-braked (PB) and 13 roll-formed (RF) specimens. Residual stresses are idealized as a summation of two types: flexural and membrane (Fig. 8). This idealization is a pragmatic rather than scientific choice. Analytical models show more complex variation through the thickness [19]. Experimental evidence from thicker bent plates support the more complicated theoretical distributions [3]. However, experimentally measuring the through thickness residual stress variation of a thin plate is infeasible. The only

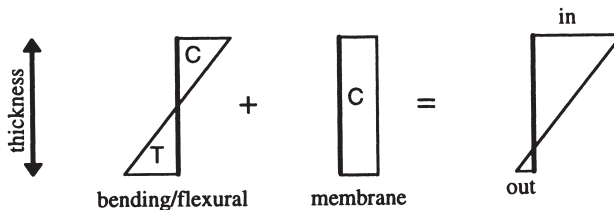


Fig. 8. Definition of flexural and membrane residual stress.

Table 2
Membrane residual stress as $\%f_y$

Element	Roll-formed		Press-braked	
	Mean	Variance	Mean	Variance
Corners	6.8	1.1	5.2	0.4
Edge stiffened	3.9	1.0	0.9	1.0
Lip	7.9	1.5	0.2	0.3
Stiffened	-1.7	1.2	0.9	0.1

available experimental measurements for thin plates ($O \sim 1$ mm) are at the faces of the plate.

4.1. Membrane residual stresses

Statistical results for membrane residual stresses are summarized in Table 2. The data is grouped by elements where the residual stresses are measured: corners, edge stiffened element, lips and stiffened elements. Membrane residual stresses are more prevalent in roll-formed members than press-braked.

Compression, membrane residual stresses cause a direct loss in compressive strength. Significant membrane residual stresses exist primarily in corner regions. Opposing this effect, the yield stress (f_y) is elevated in corner regions due to significant cold work of forming [20]. If large membrane residual stresses are modeled in the corners or other heavily worked zones, then increased yield stress in these regions should be modeled as well. Conversely, if membrane residual stresses are ignored, then elevation of the yield stress should not be included. More study is needed to assess how much these two effects counteract one another.

4.2. Flexural residual stress

Large magnitude flexural residual stresses are regularly observed — residual stresses equal to 50% f_y are not uncommon. Measured flexural residual stresses also show a large degree of variation. Statistics for flexural residual stress are reported in Table 3. Histograms and CDFs of the flexural residual stress are shown in Fig. 10.

Table 3
Flexural residual stress as $\%f_y$

Element	Roll-formed		Press-braked	
	Mean	Variance	Mean	Variance
Corners	26.8	5.0	32.7	3.3
Edge stiffened	23.5	1.0	8.0	2.5
Lip	6.7	6.4	56.0*	11.6
Stiffened	38.9	6.2	16.9	4.5

* Some lips are flame-cut, thus distorting this value.

Generally an analyst can not afford to do a series of runs with different residual stresses. Thus, average values (Fig. 9) or discrete values estimated from the CDFs (Fig. 10) are employed. A conservative approximation of residual stress magnitude may be obtained by using the CDFs. For a roll-formed section, 95% of the residual stresses are lower than $0.67f_y$ in a corner, lower than $0.43f_y$ in an edge stiffened element, and lower than $0.71f_y$ in a stiffened element. For a press-braked section the values are $0.56f_y$ in a corner, $0.40f_y$ in an edge stiffened element, and $0.53f_y$ in a stiffened element.

5. Examples

The influence of modeling assumptions such as imperfections and residual stresses is best illustrated by example. Finite strip analysis of a common cold-formed steel flexural member exhibits three elastic buckling modes (Fig. 11). For a laterally braced member the local and distortional modes are of significant concern. In the examples here, an idealized model of the compression flange (Fig. 12) is employed to isolate the elastic behavior to local and distortional buckling.

Material and geometric nonlinear finite element analysis is conducted using ABAQUS. Nine node shell elements with five integration points through the thickness are employed for modeling the section. The material is modeled as elastic–plastic with strain hardening. Detailed discussion of the FEM analysis and related work may be found elsewhere [16].

5.1. Modal imperfections

Modal imperfections refer to imperfection patterns in which the perfect geometry is perturbed using the eigenmode shapes. An idealized flange (Fig. 12) with a width

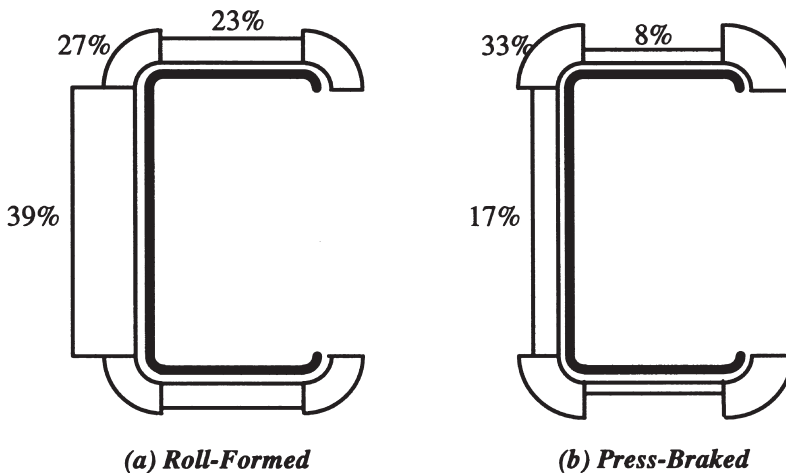


Fig. 9. Average bending residual stress as $\%f_y$.

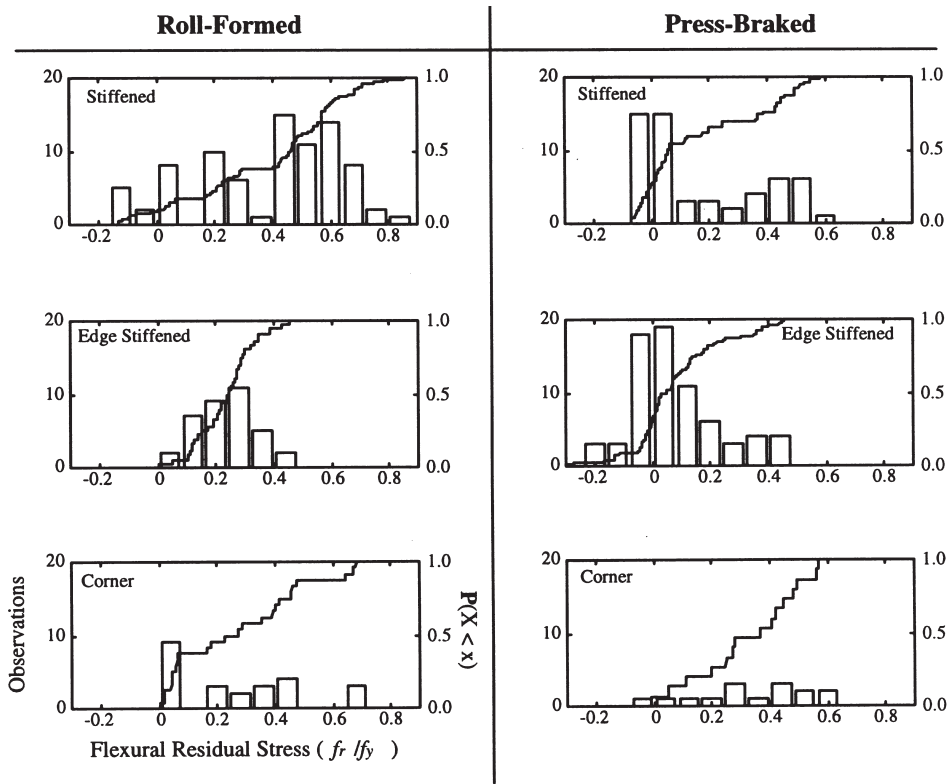


Fig. 10. Histograms and CDFs for flexural residual stress.

of 60 mm, a 90° turned down lip with a length of 10 mm and a thickness of 1 mm is investigated. Imperfection magnitudes are determined from Table 1 with $P(\Delta < d) = 0.75$. The elastic buckling load is $0.84P_y$ for local buckling and $1.04P_y$ for distortional buckling (where P_y is the yield, or squash load).

The $P-\delta$ (ultimate strength versus out of plane displacement) results indicate that use of only the local or the distortional eigenmode for the imperfection pattern is unconservative (Fig. 13). However, in this case either modal imperfection triggers the same final mechanism. This ability to reach the same final mechanism regardless of initial imperfection is not guaranteed. The final failure mechanism is consistent with the distortional eigenmode.

5.2. Generalized imperfections

The imperfection spectrum is used to generate five artificial imperfection signals (X). The signals are normalized to a maximum magnitude of 1 (X). The normalized signals are then scaled to maximum magnitudes from Table 1 and mapped onto the geometry as shown in Fig. 14. Flange width is 60 mm, lip length is 12 mm, and

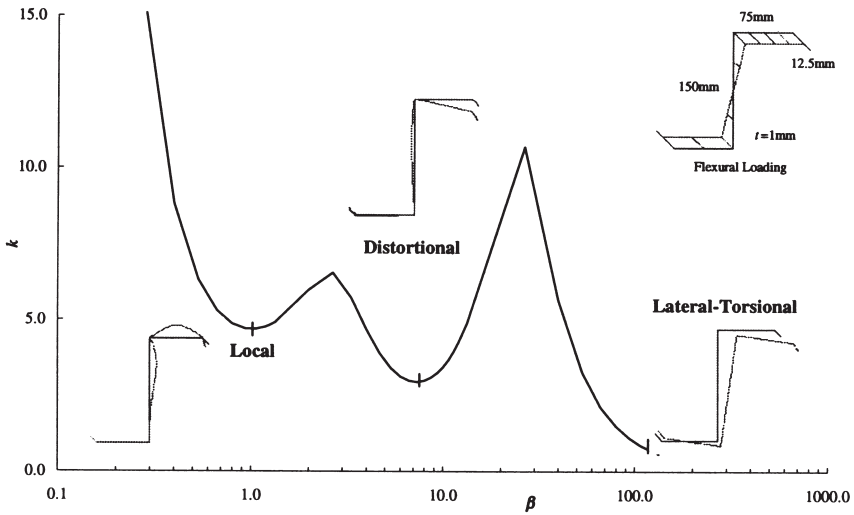


Fig. 11. Finite strip analysis results.

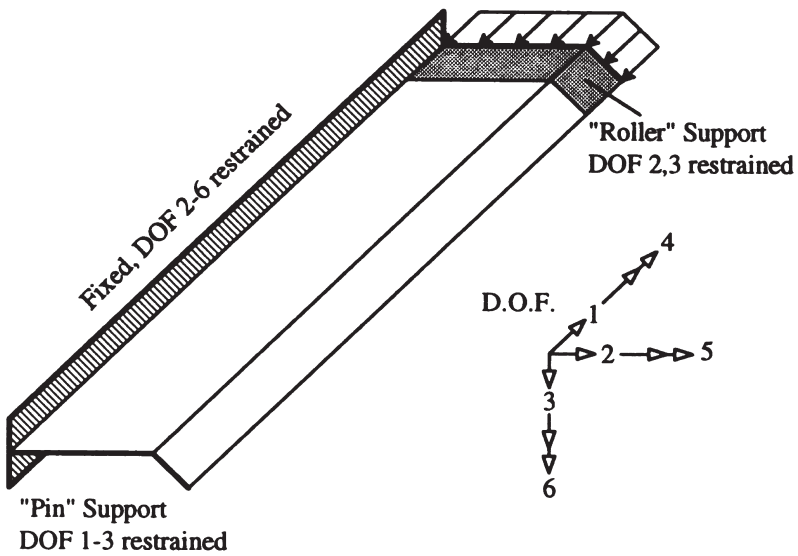


Fig. 12. Boundary conditions.

thickness is 1 mm. The elastic local buckling load is $0.85P_y$, and distortional buckling is $1.25P_y$.

Table 4 summarizes the analysis results for the five different imperfection patterns (seeds) and the four different imperfection magnitudes ($P(\Delta < d)$). Conclusions from modeling generalized imperfections are more complicated than those from modal imperfections. Greater loss in strength and increased variability both occur as the

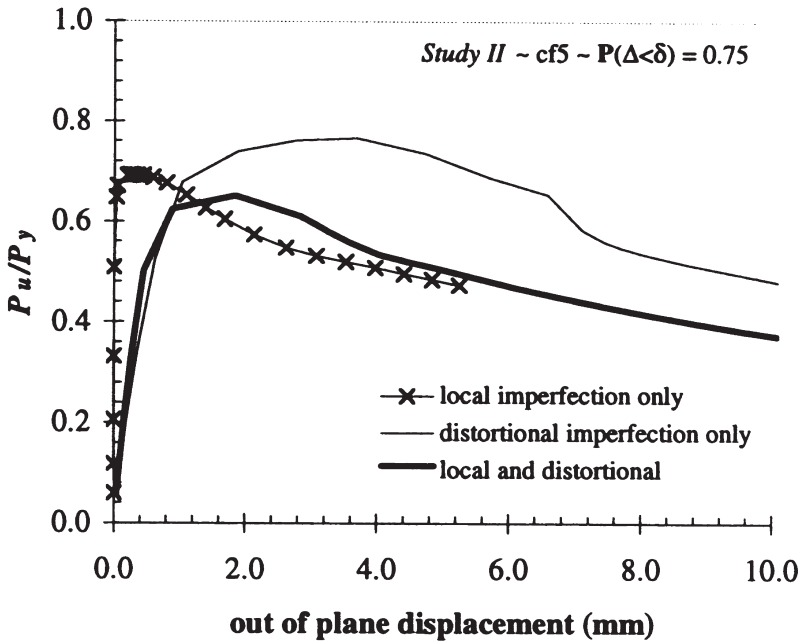


Fig. 13. Load–displacement curve.

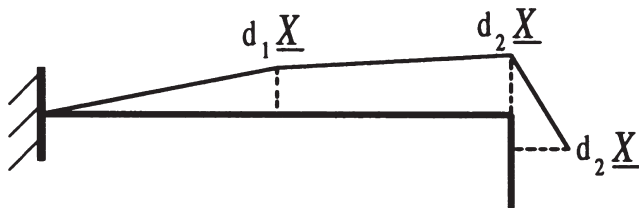


Fig. 14. Spatial mapping of X.

imperfection magnitude is increased. Strength loss is more pronounced than increased variability in strength.

Modal imperfection analysis of this same example shows failure mechanisms consistent with either the local or distortional mode depending on imperfection magnitude. Analysis using generalized imperfections shows that failure is dependent on magnitude and on distribution of imperfections. For instance, realization 3 (seed 3) fails in a local mechanism in all analyses. This is due to a pronounced imperfection frequency content near the local mode for this particular realization.

Qualitatively, failure mode and yielding in a generalized imperfection analysis is different than a modal imperfection analysis. Formation of a failure mechanism in modal imperfection analysis is relatively regular. For instance, all distortional failures initiate at the crest of the midspan distortional wave. With general imperfection distri-

Table 4
Strength results with artificially generated imperfection patterns

Seed	$P(\Delta < d) = 0.25$		$P(\Delta < d) = 0.50$		$P(\Delta < d) = 0.75$		$P(\Delta < d) = 0.95$	
	P_u/P_y	Failure	P_u/P_y	Failure	P_u/P_y	Failure	P_u/P_y	Failure
1	0.72	local	0.67	dist.	0.61	dist.	0.50	dist.
2	0.74	dist.	0.70	local	0.64	dist.	0.54	dist.
3	0.71	local	0.66	local	0.59	local	0.47	local
4	0.73	dist.	0.68	dist.	0.62	dist.	0.52	dist.
5	0.72	dist.	0.68	dist.	0.62	dist.	0.53	dist.
Average	0.72		0.68		0.62		0.51	
St. dev.	0.012		0.016		0.020		0.028	
Max/min	1.05		1.07		1.09		1.15	
Range	0.03		0.04		0.05		0.07	

butions, yielding and final failure mechanisms may occur at a variety of locations. Eventually (at large deflections) a mechanism consistent with one of the eigenmodes forms. The observed failure pattern in a general imperfection analysis is more consistent with experimental observation.

5.3. Residual stresses

Inclusion of flexural residual stress has a significant qualitative effect on the solution. Consider Fig. 15 which shows the locations that are yielding at the ultimate load for the example. Significant yielding in the bottom is due to the compression

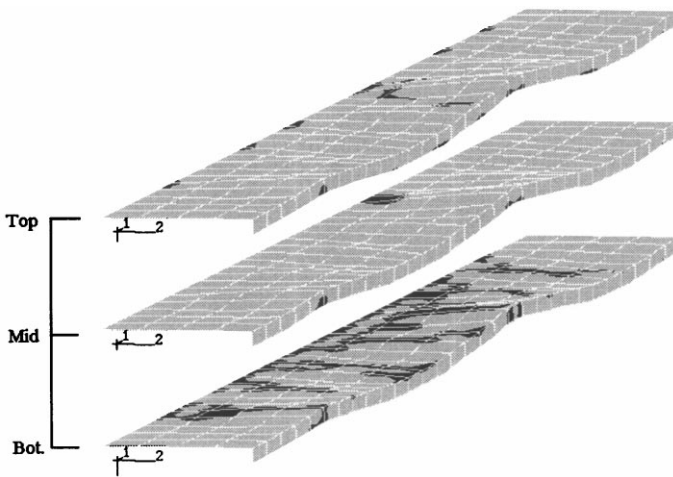


Fig. 15. von Mises stress $> f_y$ at different locations through the thickness.

portion of the flexural residual stress. If the residual stress is ignored the yielding locations do not have this level of complexity.

The primary importance of residual stresses is in how load is carried, not in final magnitude. Flexural residual stresses are self-equilibrating through the thickness and thus have a small net effect. However, early yielding on the face of the plates has a strong influence on stress distribution and on interpretations of the way the load is carried in the plate.

6. Modeling suggestions

The most robust way to assess the influence of geometric imperfections and residual stresses is to perform a direct probabilistic simulation considering both distribution and magnitude as random quantities. Even in ideal circumstances this approach is typically not selected due to the large amount of analyses required. Options for more practical study of these quantities follow.

6.1. Imperfections

6.1.1. Limited study

Employ at least two fundamentally different eigenmode shapes summed together for the imperfection distribution. Do not sum two modes together which are actually the same fundamental mode, but at a different wavelength. Select imperfection magnitudes from the simple rules of thumb or more conservative magnitudes from Table 1.

If at least two analyses can be conducted select a range of imperfection magnitudes from Table 1. For instance cover the middle 50% by using values for $\mathbf{P}(\Delta < d) = 25$ and 75%. This method allows imperfection sensitivity to be indirectly addressed.

6.1.2. General study

If modal imperfections are used then a range of imperfection magnitudes should be investigated. (Values from Table 1 are a good start.) A more complete solution would use the imperfection spectrum to generate artificial imperfections along the length and values from Table 1 to scale the magnitude. Several analyses may be required to generate sufficient information about the variation of the strength.

6.2. Residual stresses

6.2.1. Limited study

If detailed corner information is not of concern, then membrane residual stresses may be ignored. Flexural residual stresses should be modeled in all elements. For the magnitude use average values (Fig. 9) or more conservative estimates from Fig. 10.

6.2.2. General study

Model membrane and flexural residual stresses. Increase the yield stress in the corner and other highly worked zones where membrane residual stresses are elevated. Select magnitudes from Fig. 10 and perform a minimum of two analyses to assess the influence of varying residual stress.

7. Conclusions

Characterization of geometric imperfections and residual stresses in cold-formed steel members is possible. Existing data on imperfections provides a limited but useful characterization of imperfection magnitude. Imperfection distributions are assessed via a pilot experimental program and the concept of an imperfection spectrum is introduced. The use of the imperfection spectrum for modal imperfections and generalized imperfections is explained. Data on residual stresses provide insight into appropriate selection of distribution and magnitude. Examples using nonlinear finite element analysis demonstrate how imperfection magnitude, imperfection distribution and residual stresses all influence the solution results.

A great deal of complexity is required for computational modeling of the ultimate strength of cold-formed steel members. Comparison of results among analysts as well as the reliability of the solution itself requires a greater consensus on the inputs used in the modeling process. To this end, geometric imperfections and residual stresses are examined with the hope of determining practical distributions and magnitudes for use in modeling. A simple set of guidelines are presented as a first step towards this goal.

References

- [1] Avery P, Mahendran M. Finite element analysis of hollow flange beams with web stiffeners. Proceedings of the Thirteenth International Specialty Conference on Cold-formed Steel Structures, St. Louis, Missouri, 1996.
- [2] Davies JM, Jiang C. Design of profiled metal sheeting and decking. Proceedings of the Third International Conference on Steel and Aluminum Structures, Istanbul, Turkey, 1995.
- [3] Key PW, Hancock GJ. A theoretical investigation of the column behavior of cold-formed square hollow sections. *Thin-walled Structures* 1993;16(1/4):31–64.
- [4] Lau SCW. Distortional buckling of thin-walled columns. Ph.D. dissertation, University of Sydney, Sydney, Australia, 1988.
- [5] Lucas RM, Al-Bermani FGA, Kitipornchai S. Modeling of cold-formed purlins-sheeting systems. Proceedings of the Thirteenth International Specialty Conference on Cold-formed Steel Structures, St. Louis, Missouri, 1996.
- [6] Sümer O. Behavior of thin-walled members with single intermediate stiffeners, based on numerical analysis. Proceedings of the Third International Conference on Steel and Aluminum Structures, Istanbul, Turkey, 1995.
- [7] Bernard ES. Flexural behavior of cold-formed profiled steel decking. Ph.D. dissertation, University of Sydney, Sydney, Australia, 1993.
- [8] Dat DT, Peköz T. The strength of cold-formed steel columns. Department of Structural Engineering Report, Cornell University, Ithaca, New York, 1980.

- [9] Ingvarsson L. Cold-forming residual stresses and box columns built up by two cold-formed channel sections welded together *Bulletin of the Department of Building Statics and Structural Engineering* 1977, **121**, The Royal Institute of Technology, Stockholm, Sweden.
- [10] Kwon YB. Post-buckling behavior of thin-walled channel sections. Ph.D. dissertation, University of Sydney, Sydney, Australia, 1992.
- [11] Mulligan GP. The influence of local buckling on the structural behavior of singly symmetric cold-formed steel columns. Ph.D. dissertation, Cornell University, Ithaca, New York, 1983.
- [12] Thomasson P. Thin-walled C-shaped panels in axial compression. *Swedish Council for Building Research* 1978;D1:1978.
- [13] Schafer BW, Grigoriu M, Peköz T. A probabilistic examination of the ultimate strength of cold-formed steel elements. *Proceedings of the Thirteenth International Specialty Conference on Cold-formed Steel Structures*, St. Louis, Missouri, 1996.
- [14] Lin YK. *Probabilistic Theory of Structural Dynamics*. Robert E. Krieger Publishing, Melbourne, FL, 1996.
- [15] Soong TT, Grigoriu M. *Random Vibration of Mechanical and Structural Systems*. Prentice Hall, Englewood Cliffs, 1993.
- [16] Schafer BW. Cold-formed steel behavior and design: analytical and numerical modeling of elements and members with longitudinal stiffeners. Ph.D. dissertation, Cornell University, Ithaca, New York, 1997.
- [17] De Batista EM, Rodrigues FC. Residual stress measurements on cold-formed profiles. *Experimental Techniques* 1992;16(5):25–9.
- [18] Weng CC. Flexural buckling of cold-formed steel columns. Ph.D. dissertation, Cornell University, Ithaca, New York, 1987.
- [19] Rondal J. Residual stresses in cold-rolled profiles. *Construction and Building Material* 1987;1(3):0–0.
- [20] Karren KW. Effects of cold-forming on light-gage steel members. Ph.D. dissertation, Cornell University, Ithaca, New York, 1965.